

Gluino Search with Stop and Top in Nonuniversal Gaugino Mass Models at LHC and Future Colliders

Zafer Altın^{a1}, Ali Çiçi^{a2}, Zerrin Kirca^{a3}, Qaisar Shafi^{b4} and Cem Salih Ün^{a5}

^a*Department of Physics, Bursa Uludağ University, TR16059 Bursa, Turkey*

^b*Bartol Research Institute, Department of Physics and Astronomy, University of
Delaware, Newark, DE 19716, USA*

Abstract

We discuss the gluino mass in the CMSSM and Nonuniversal Gaugino Mass Models (NUGM) frameworks in light of the results from the current LHC and Dark Matter experiments. Assuming negative results from the current and near future LHC experiments, we probe the gluino mass scales by considering its decay modes into stop and top quarks, $\tilde{g} \rightarrow \tilde{t}_1 t$ and $\tilde{g} \rightarrow \bar{t} t \tilde{\chi}_1^0$, where $\tilde{t}_1 t$ represents both $\tilde{t}_1 \bar{t}$ and $\tilde{t}_1^* t$. The region with $m_{\tilde{g}} \lesssim 2$ TeV is excluded up to 68% CL in the CMSSM if the gluino decays into a stop and top quark, while the 95% CL exclusion requires $m_{\tilde{g}} \gtrsim 1.9$ TeV. Considering an error of about 10% in calculations of the SUSY mass spectrum, such exclusion bounds on the gluino mass more or less overlap with the current LHC results. The decay mode $\tilde{g} \rightarrow \bar{t} t \tilde{\chi}_1^0$ may take over if $\tilde{g} \rightarrow \tilde{t}_1 t$ is not allowed. One can probe the gluino mass in this case up to about 1.5 TeV with 68% CL in the CMSSM, and about 1.4 TeV with 95% CL. Imposing the Dark Matter constraints yields a lower bound on the gluino and stop masses of about 3.2 TeV from below, which is beyond the reach of the current LHC experiments. A similar analyses in the NUGM framework yield exclusion curves for the gluino mass $m_{\tilde{g}} \gtrsim 2.1$ TeV at 14 TeV for both decay modes of the gluino under consideration. We also show that increasing the center of mass energy to 27 TeV can probe the gluino mass up to about 3 TeV through its decay mode into stop and top quark. The Dark Matter constraints are not very severe in the framework of NUGM, and they allow solutions with $m_{\tilde{g}}, m_{\tilde{t}} \gtrsim 1$ TeV. In addition, with NUGM the LSP neutralino can coannihilate with gluino and/or stop for $m_{\tilde{g}}, m_{\tilde{t}} \approx m_{\tilde{\chi}_1^0} \in [0.9 - 1.5]$ TeV. With the 100 TeV FCC collider one can probe the gluino masses up to about 6 TeV with 36.1 fb^{-1} integrated luminosity. We also find that the decay $\tilde{g} \rightarrow \bar{t} t$ can indirectly probe the stop mass up to about 4 TeV.

¹E-mail: 501407009@ogr.uludag.edu.tr

²E-mail: 501507007@ogr.uludag.edu.tr

³E-mail: zkirca@uludag.edu.tr

⁴shafi@bartol.udel.edu

⁵E-mail: cemsalihun@uludag.edu.tr

1 Introduction

The low scale implications of Supersymmetric (SUSY) SO(10) grand unified theories (GUTs) such as third family Yukawa unification and sparticle spectroscopy in SO(10) [1, 2] and SU(5) [3] have occupied a fair amount of attention in recent years. The current LHC results exclude a gluino lighter than about 2.1 TeV [5], unless it happens to be the Next to Lightest Supersymmetric Particle (NLSP), in which case the bound on its mass can go down about 800 GeV. The bound on the stop mass varies depending on its decay modes. Thus, $m_{\tilde{t}} \gtrsim 1200$ GeV if $\tilde{t} \rightarrow t\tilde{\chi}_1^0$ and $m_{\tilde{t}} \gtrsim 1100$ GeV for $\tilde{t} \rightarrow b\tilde{\chi}_1^\pm$ [6]. These analyses have been performed mostly for low scale SUSY, where the SUSY spectrum can be adjusted such that the particles participating in the analyzed decay modes are light enough, while the rest of the spectrum is appropriately heavy and cannot interfere in the stop and gluino decays. Since a generic supersymmetric model has more than a hundred free parameters, such assumptions seem plausible. Besides, the probability for the relevant decay modes under the analyses (branching fractions, for instance) can be optimized.

On the other hand, the SUSY GUTs SO(10) and SU(5) can significantly reduce the number of free parameters, and some of the low scale assumptions may not be possible, when all low scale observables are calculated in terms of a few free parameters. For instance, one of our recent studies has shown that the solutions with $m_{\tilde{t}} \lesssim 500$ GeV can be excluded only within 60% confidence level (CL) for $\tilde{t} \rightarrow t\tilde{\chi}_1^0$, and at 50% CL for $\tilde{t} \rightarrow b\tilde{\chi}_1^\pm$ [7]. For $m_{\tilde{t}} \gtrsim 500$ GeV the exclusion is realized at the order of a few percent, even though the current results exclude a stop mass below about 800 GeV, if these decay modes are allowed in the low scale analyses.

A similar discussion can be applied to the gluino. The current results exclude solutions with $m_{\tilde{g}} \lesssim 2.4$ TeV, when the LSP neutralino is of mass around a TeV, while the mass bound on the gluino is reduced to about 2.2 TeV, as the LSP neutralino mass decreases [6]. Even though the sleptons and/or sneutrinos are light enough to take part, the lower mass bound on the gluino is still about 2 TeV [8]. A 125 GeV Higgs boson mass constrains the stop masses at around a TeV scale from below, but it is still possible to include the stop in the gluino decay mode $\tilde{g} \rightarrow \tilde{t}t$. If this decay mode is kinematically allowed, the bound on the gluino mass can be lowered to about 1.8 TeV [9], while it has recently been reported by the CMS analyses as $m_{\tilde{g}} \gtrsim 1.6$ TeV [6].

In this study, we consider the gluino decay into a stop and top quark, and apply the constraints from low scale analyses. Since the sbottom usually happens to be much heavier than stops (see, for instance, the benchmark points represented in several papers in Ref. [2]), we do not consider processes in which the gluino decays into a sbottom and bottom quarks. Hence, the decay cascades considered are the following:

$$pp \rightarrow \tilde{g}\tilde{g} \xrightarrow{\tilde{g} \rightarrow \tilde{t}t} \tilde{t}\tilde{t}^*t\bar{t} \xrightarrow{\tilde{t} \rightarrow t\tilde{\chi}_1^0} t\bar{t}t\tilde{\chi}_1^0\tilde{\chi}_1^0, \quad (1)$$

$$pp \rightarrow \tilde{g}\tilde{g} \xrightarrow{\tilde{g} \rightarrow \tilde{t}t} \tilde{t}\tilde{t}^*t\bar{t} \xrightarrow{\tilde{t} \rightarrow b\tilde{\chi}_1^\pm} b\bar{b}t\tilde{\chi}_1^\pm\tilde{\chi}_1^\pm \xrightarrow{\tilde{\chi}_1^\pm \rightarrow W^\pm\tilde{\chi}_1^0} b\bar{b}t\tilde{W}^\pm W^\pm\tilde{\chi}_1^0\tilde{\chi}_1^0. \quad (2)$$

The process given in Eq.(1) will be called Signal1, while Signal2 refers to the process given in Eq.(2). If the gluino decay mode involving a stop and top quarks is not likely, then one can consider another mode denoted as Signal3, in which the gluino decays directly into a LSP neutralino along with a pair of top quarks:

$$pp \rightarrow \tilde{g}\tilde{g} \xrightarrow{\tilde{g} \rightarrow \bar{t}t\tilde{\chi}_1^0} \bar{t}t\bar{t}t\tilde{\chi}_1^0\tilde{\chi}_1^0. \quad (3)$$

As in the low scale analyses, we start with the gluino pair production and the next step of the decay cascade includes one pair of stops and one pair of top quarks. After this step, the analyses may resemble the stop quark analyses, where the stop can decay through either of the two processes, $\tilde{t} \rightarrow t\tilde{\chi}_1^0$ and $\tilde{t} \rightarrow b\tilde{\chi}_1^\pm$. The strongest constraint in the latter case arises if the chargino is allowed to decay into a LSP neutralino and a W^\pm boson. Note that it is also possible that the stop can decay into a charm quark and LSP neutralino; however, the signal is soft in this case, and the constraint is not very severe ($m_{\tilde{t}} \gtrsim 230$ GeV [10]). Thus, we do not consider this latter case in the following discussion. The processes given above continue with the decays such as $t \rightarrow bW^\pm$ and $W^\pm \rightarrow l\nu$.

The third stage (fourth in the process given in Eq.(2)) in the decay cascade of the signal includes two pairs of the third family quarks and two LSP neutralinos, if the stop decays into a top quark and LSP neutralino. The second option involves two W-bosons, and pairs of top and bottom quarks along with two neutralinos. The relevant background processes can be listed as $t\bar{t}$, single top, $t\bar{t}W$, $t\bar{t}Z$, $t\bar{t}t\bar{t}$, $t\bar{t}h$, WW , WZ , ZZ and W/Z + jets [9]. Even though the top quark pair production dominates in the background processes, the signal is expected to have much more missing energy, and the events from the top pair production background can be suppressed by applying a cut on the missing energy as $\cancel{E}_T \gtrsim 300$ GeV [7]. In this case, production of two pairs top quarks can be considered the main background in its final state.

Following [7], as a benchmark study, our aim here is to explore the gluino searches in the framework of SUSY GUTs via the decay mode $\tilde{g} \rightarrow \bar{t}t$. The analyses of [7] will be generalized by employing the constraints and calculations to the whole data generated within the SUSY GUT framework. The paper is organized as follows. Section 2 summarizes the scanning procedure and the experimental constraints employed in our analyses. In Section 3 we briefly present the results and constraints on the gluino mass in CMSSM. Since the universal boundary conditions of CMSSM lead to a linear correlation between the gluino and LSP neutralino masses, we generalize our discussion in Section 4 by allowing non-universal gaugino masses (NUGM) at the GUT scale. We describe the constraints on the gluino mass from the current LHC experiments, as well as from the High Energy LHC (HE-LHC at 27 TeV) and Future Circular Collider (FCC at 100 TeV). Our conclusions are summarized in Section 5.

2 Scanning Procedure and Experimental Constraints

We have employed SPheno 4.0.3 package [11, 12] generated with SARAH 4.13.0 [13, 14]. In this package, the weak scale values of the gauge and Yukawa couplings in MSSM are evolved to the unification scale M_{GUT} via the renormalization group equations (RGEs). M_{GUT} is determined by the requirement of unification of the gauge couplings through their RGE evolutions. Note that we do not strictly enforce the unification condition $g_1 = g_2 = g_3$ at M_{GUT} since a few percent deviation from the unification can be assigned to unknown GUT-scale threshold corrections [15, 16]. With the boundary conditions given at M_{GUT} , all the soft supersymmetry breaking (SSB) parameters along with the gauge and Yukawa couplings are evolved back to the weak scale.

We have performed random scans over the parameter space of CMSSM and NUGM models as follows:

CMSSM	NUGM
$0 \leq m_0 \leq 5 \text{ (TeV)}$	$0 \leq m_0 \leq 5 \text{ (TeV)}$
$0 \leq M_{1/2} \leq 5 \text{ (TeV)}$	$0 \leq M_1, M_2, M_3 \leq 5 \text{ (TeV)}$
$1.2 \leq \tan \beta \leq 50$	$1.2 \leq \tan \beta \leq 50$
$-3 \leq A_0/m_0 \leq 3$	$-3 \leq A_0/m_0 \leq 3$

(4)

where m_0 is the universal SSB mass term for the matter scalars and Higgs fields. M_1 , M_2 and M_3 are the SSB mass terms for the gauginos associated with the $U(1)_Y$, $SU(2)_L$ and $SU(3)_C$ symmetry groups respectively. While the SSB gaugino masses are independent terms in NUGM, in CMSSM they satisfy $M_1 = M_2 = M_3 = M_{1/2}$ at M_{GUT} . A_0 is the SSB trilinear coupling, and $\tan \beta$ is ratio of VEVs of the MSSM Higgs doublets. In addition to these parameters, the radiative electroweak symmetry breaking (REWSB) conditions determine the value of the MSSM μ -term but not its sign, which we assume to be positive in our scans. Finally, we have used the central value of top quark mass, $m_t = 173.3 \text{ GeV}$ [17]. Note that the sparticle spectrum is not too sensitive for one or two sigma variation in the top quark mass [18], but it can shift the Higgs boson mass by 1-2 GeV [19, 20].

The REWSB condition provides a strict theoretical constraint [21, 22, 23, 24, 25] over the fundamental parameter space given in Eq.(4). Another important constraint comes from the relic abundance of charged supersymmetric particles [26]. This constraint excludes regions which yield charged particles such as stop and stau as the lightest supersymmetric particle (LSP). In this context, we accept only the solutions which satisfy the REWSB condition and yield neutralino LSP. In this case, it is also appropriate that the LSP becomes a suitable dark matter candidate. The thermal relic abundance of LSP should, of course, be consistent with the current results from the WMAP [27] and Planck [28] satellites. However, even if a solution does not satisfy the dark matter observations, it can still survive in conjunction with other form(s) of the dark matter [29]. We mostly focus on the LHC allowed solutions, but we also discuss the DM implications in our results.

In scanning the parameter space we use an interface, which employs the Metropolis-Hasting algorithm described in [38, 39]. After generating the low scale data with SPheno, all outputs are transferred to MicrOmegas [30] for calculations of the relic abundance of the LSP neutralino as a candidate for DM. At the final step, we transfer the same output files to MadGraph [31] to calculate the cross-sections of the signal and relevant background processes. We should note that the following approximation has been used in the cross-section calculations:

$$\sigma(\text{Signal1}) \approx \sigma(pp \rightarrow \tilde{g}\tilde{g}) \times \text{BR}(\tilde{g} \rightarrow \tilde{t}_1 t) \times \text{BR}(\tilde{t}_1 \rightarrow t \tilde{\chi}_1^0)^2, \quad (5)$$

$$\sigma(\text{Signal2}) \approx \sigma(pp \rightarrow \tilde{g}\tilde{g}) \times \text{BR}(\tilde{g} \rightarrow \tilde{t}_1 t) \times \text{BR}(\tilde{t}_1 \rightarrow b \tilde{\chi}_1^\pm)^2 \times \text{BR}(\tilde{\chi}_1^\pm \rightarrow W^\pm \tilde{\chi}_1^0)^2, \quad (6)$$

$$\sigma(\text{Signal3}) \approx \sigma(pp \rightarrow \tilde{g}\tilde{g}) \times \text{BR}(\tilde{g} \rightarrow \bar{t} t)^2. \quad (7)$$

Even though MadGraph calculates cross-sections by using full matrix elements, comparisons over a control set of data points reveal an error of 0.7% at most between the MadGraph results and the approximations given above. Thus, we obtain the results for the gluino pair production by MadGraph, and the full cross-section of the signals are

calculated by using the approximation in Eqs.(5, 6 and 7). After collecting the MadGraph results, we successively apply the mass bounds on all sparticles [32] and the constraints from the rare B-decays ($B_s \rightarrow \mu^+\mu^-$ [33], $B_s \rightarrow X_s\gamma$ [34] and $B_u \rightarrow \tau\nu_\tau$ [35]). In applying the mass bounds on the supersymmetric particles, we apply the LEP II bound on the gluino [36]. The solutions surviving after these constraints are referred to as the LHC allowed points, and the DM constraints are applied on these solutions. Regarding the relic abundance of LSP neutralino, we show bounds both from the WMAP and Planck satellites within 5σ uncertainty.

The experimental constraints can be listed as follows:

$$\begin{aligned}
123 &\leq m_h \leq 127 \text{ GeV} \\
m_{\tilde{g}} &\geq 260 \text{ GeV} \\
0.8 \times 10^{-9} &\leq BR(B_s \rightarrow \mu^+\mu^-) \leq 6.2 \times 10^{-9} \text{ (} 2\sigma \text{)} \\
2.9 \times 10^{-4} &\leq BR(b \rightarrow s\gamma) \leq 3.87 \times 10^{-4} \text{ (} 2\sigma \text{)} \\
0.15 &\leq \frac{BR(B_u \rightarrow \nu_\tau\tau)_{MSSM}}{BR(B_u \rightarrow \nu_\tau\tau)_{SM}} \leq 2.41 \text{ (} 3\sigma \text{)} \\
0.0913 &\leq \Omega h^2(\text{WMAP}) \leq 0.1363 \text{ (} 5\sigma \text{)} \\
0.114 &\leq \Omega h^2(\text{Planck}) \leq 0.126 \text{ (} 5\sigma \text{)} .
\end{aligned} \tag{8}$$

In addition to these constraints, we define the signal significance (SS) as

$$SS = \frac{S}{\sqrt{S+B}} , \tag{9}$$

where S and B refer to the event number (cross-section \times Luminosity) of the signal and background respectively. We use the following correspondence to translate SS to the confidence level (CL) [37]:

$$\begin{aligned}
0 \leq SS < 1 &\rightarrow \text{hardly excluded} , \\
1 \leq SS < 2 &\rightarrow \text{excluded up to 68\%} , \\
2 \leq SS < 3 &\rightarrow \text{excluded up to 95\%} .
\end{aligned} \tag{10}$$

3 CMSSM at 14 TeV

We first discuss the results for the possible signal processes given in Eqs.(1, 2 and 3) in the CMSSM framework, and compare with the current LHC results on the gluino mass scale to see if there is any difference. The CMSSM boundary conditions imposed at M_{GUT} yield a universal SSB mass term $M_{1/2}$ for all MSSM gauginos; hence, $M_{1/2}$ determines both the LSP neutralino and gluino masses. In this context, one expects a linear correlation between the low scale masses of the LSP neutralino and gluino. Figure 1 displays our results with plots in the $m_0 - M_{1/2}$ and $m_{\tilde{g}} - m_{\tilde{t}_1}$ planes. All points are compatible with REWSB and

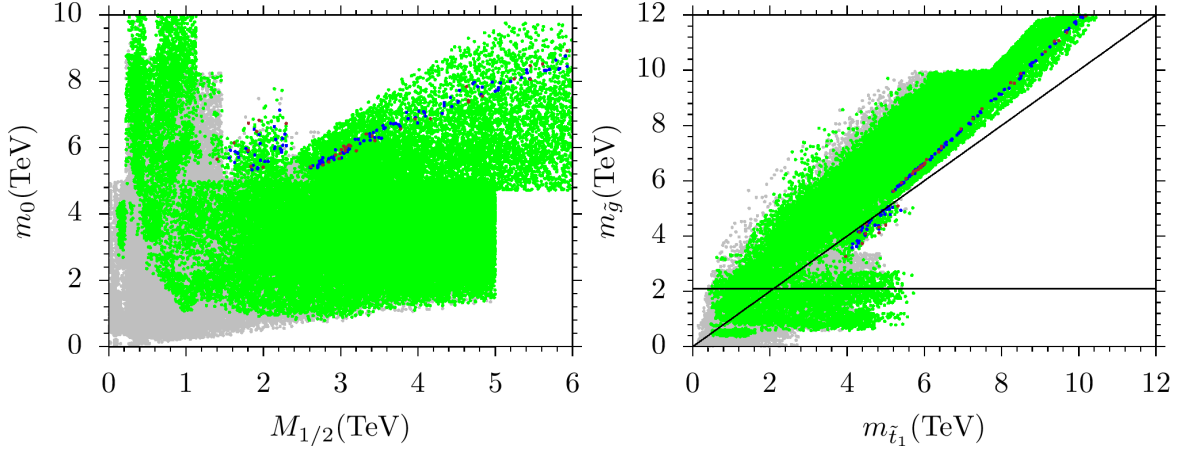


Figure 1: Plots in the $m_0 - M_{1/2}$ and $m_{\tilde{g}} - m_{\tilde{t}_1}$ planes. All points are compatible with REWSB and neutralino LSP conditions. Green points are consistent with the current mass bounds and constraints from rare B-meson decays except for gluino, on whose mass the LEP II bound is applied. Blue points form a subset of green, and they indicate the solutions allowed by the WMAP bound on the relic abundance of neutralino LSP within 5σ ; brown points are a subset of blue and they satisfy the Planck bounds on the relic abundance within 5σ . The horizontal line in the right panel indicates the current mass bound on the gluino mass, and the diagonal line indicates the mass degeneracy between the stop and gluino.

neutralino LSP conditions. Green points are consistent with the current mass bounds and constraints from rare B-meson decays except for gluino, on whose mass the LEP II bound is applied. Blue points form a subset of green, and they indicate the solutions allowed by the WMAP bound on the relic abundance of neutralino LSP within 5σ ; brown points are a subset of blue and they satisfy the Planck bounds on the relic abundance within 5σ . The horizontal line in the right panel indicates the current mass bound on the gluino mass, and the diagonal line indicates the mass degeneracy between the stop and gluino. Even though we allow relatively low values for the SSB mass terms for scalars and gauginos, a strong bound on these parameters arises from DM considerations. The WMAP and Planck bound on the relic abundance of the LSP neutralino (blue and brown points) exclude most of the solutions, especially those in regions with $m_0 \lesssim 5$ TeV and $M_{1/2} \lesssim 1.2$ TeV.

The low scale impact of the bounds on these GUT scale parameters can also be expressed in terms of gluino and stop masses as shown in the right panel of Figure 1. The $m_{\tilde{g}} - m_{\tilde{t}_1}$ plane shows that a gluino heavier than stop can be realized in much of the parameter space. The DM considerations constrain the stop and gluino masses as $m_{\tilde{t}_1}, m_{\tilde{g}} \gtrsim 4$ TeV, which is beyond the reach of the current LHC experiments at 14 TeV [40], while the near future experiments provide some hope to probe gluino and stop masses in this mass range.

We show the low scale mass spectrum for gluino, stop, LSP neutralino and the lightest chargino in Figure 2 with plots in the $m_{\tilde{g}} - m_{\tilde{\chi}_1^0}$, $m_{\tilde{t}_1} - m_{\tilde{\chi}_1^0}$, $m_{\tilde{g}} - m_{\tilde{\chi}_1^\pm}$ and $m_{\tilde{t}_1} - m_{\tilde{\chi}_1^\pm}$ planes. The color coding is the same as in Figure 1. The diagonal lines in the panels mark the region of equal masses for the particles displayed. The horizontal lines in the top left and bottom left panels indicate the current bound on the gluino mass. As expected and mentioned above, the $m_{\tilde{g}} - m_{\tilde{\chi}_1^0}$ plot reveals a linear correlation between the gluino and the LSP neutralino masses due to the universal gaugino mass term $M_{1/2}$ at M_{GUT} . As a result,

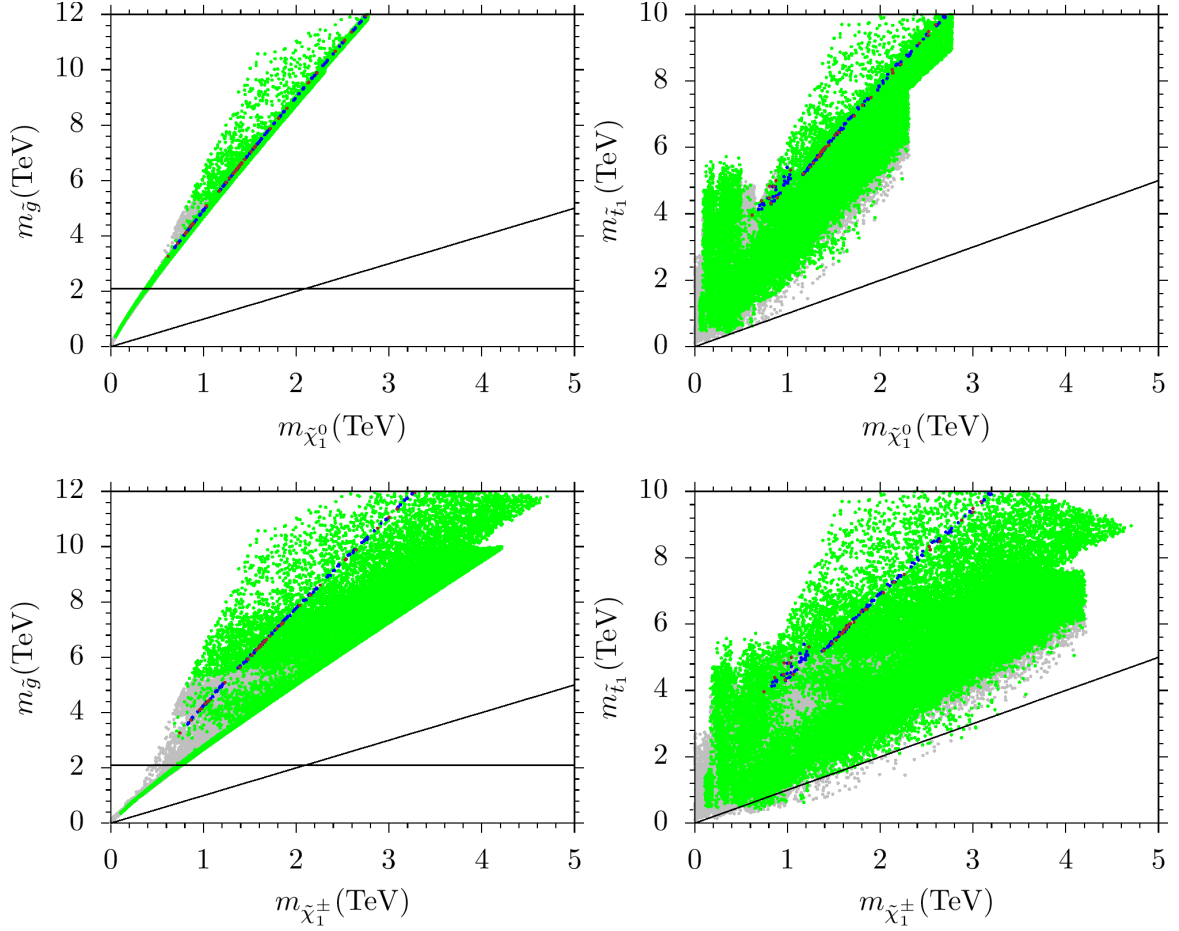


Figure 2: Plots in the $m_{\tilde{g}} - m_{\tilde{\chi}_1^0}$, $m_{\tilde{t}_1} - m_{\tilde{\chi}_1^0}$, $m_{\tilde{g}} - m_{\tilde{\chi}_1^\pm}$ and $m_{\tilde{t}_1} - m_{\tilde{\chi}_1^\pm}$ planes. The color coding is the same as in Figure 1. The diagonal lines in the panels show the degeneracy in mass states of the plotted particles. The horizontal lines in the top left and bottom left panels indicate the current bound on the gluino mass.

even though we do not apply the current gluino mass bound, CMSSM cannot yield gluino as a next to LSP (NLSP) particle in the mass spectrum. On the other hand, a gluino as heavy as about 12 TeV can be realized. Similarly, the stop can be as heavy as the gluino, while it is also possible to realize the stop as NLSP with $m_{\tilde{t}_1} \sim m_{\tilde{\chi}_1^0} \sim 500$ GeV, as is seen from the $m_{\tilde{t}_1} - m_{\tilde{\chi}_1^0}$ plot. As well as neutralino, the lightest chargino can also take part in possible signal processes, while the gluino is always much heavier than the chargino as shown in the $m_{\tilde{g}} - m_{\tilde{\chi}_1^\pm}$ plane. Similarly, the stop is heavier than the chargino in most of the parameter space, while it is also possible to realize $m_{\tilde{t}_1} \lesssim m_{\tilde{\chi}_1^\pm}$ in a small portion of the parameter space (below the diagonal line in the $m_{\tilde{t}_1} - m_{\tilde{\chi}_1^\pm}$ plane). Even though the DM constraints bound the stop and gluino masses at about 4 TeV from below, the LSP neutralino and lightest chargino masses are bounded from below at about 500 GeV, as seen from all plots in Figure 2.

The probe of solutions with a gluino lighter than the current bound (~ 2.1 TeV) depends on the strength of the signal, which is triggered with the gluino pair production, whose cross-section is shown in Figure 3 in correlation with the gluino (top left) and stop (top right) masses, $\text{BR}(\tilde{g} \rightarrow \tilde{t}_1 t)$ and $\text{BR}(\tilde{t}_1 \rightarrow t \tilde{\chi}_1^0)$. The color coding is the same as in Figure

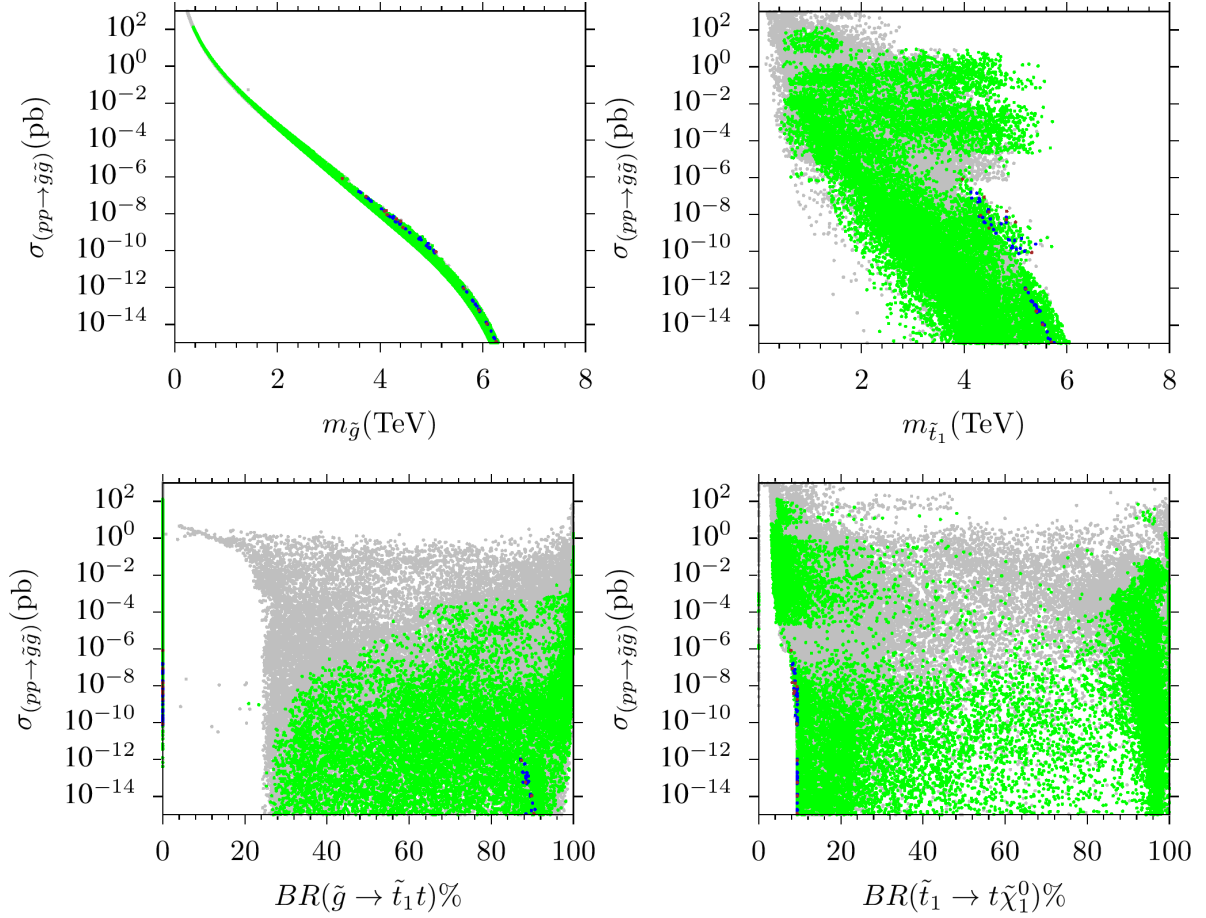


Figure 3: Plots for the gluino pair production cross-section versus the gluino mass (top left), stop mass (top right), $BR(\tilde{g} \rightarrow \tilde{t}_1 t)$ and $BR(\tilde{t}_1 \rightarrow t\tilde{\chi}_1^0)$. The color coding is the same as in Figure 1.

1. The $\sigma(pp \rightarrow \tilde{g}\tilde{g}) - m_{\tilde{g}}$ plane reveals a decreasing correlation with the gluino mass as it increases. This is expected, since the heavy masses requires greater energies, and the results represented in the $\sigma(pp \rightarrow \tilde{g}\tilde{g}) - m_{\tilde{g}}$ plane are consistent with the results previously obtained [41, 42]. According to our results, the gluino pair production can be realized as high as about 100 pb if its mass is about $\mathcal{O}(100\text{GeV})$, while it drops to about 10^{-2} pb if the gluino mass is of order a TeV. The DM constraints lower the cross-section further to about 10^{-6} pb for $m_{\tilde{g}} \gtrsim 3.2$ TeV. The production is not likely ($\sigma(pp \rightarrow \tilde{g}\tilde{g}) \ll 10^{-5}$ pb) for $m_{\tilde{g}} \gtrsim 5$ TeV. Even though the correlation is not as sharp as that with the gluino mass, the heavy stop mass scales also exhibit an inverse correlation with the gluino pair production cross-section, as seen in the $\sigma(pp \rightarrow \tilde{g}\tilde{g}) - m_{\tilde{t}_1}$ plane. Similarly the gluino pair production is not likely for $m_{\tilde{t}_1} \gtrsim 5$ TeV. The bottom panels show the possibility of the gluino and stop decays in terms of the branching fractions of the relevant processes. It is possible to find solutions in which $BR(\tilde{g} \rightarrow \tilde{t}_1 t) \approx 100\%$, while the DM constraints reduce it down to about 90%. The last panel shows how likely the stop can decay into a LSP neutralino along with a top quark, which provides the strongest exclusion on the stop mass. Even though it is possible to realize it as 100%, it can only be as high as about 10% when the DM constraints are applied.

Another possibility is for the stop to decay into the lightest chargino along with a bottom quark. In turn, the chargino decays into the LSP neutralino and a W -boson. Figure 4 represents the results for the cross-section of the gluino pair production and stop decay channels involving bottom and chargino (left), bottom, W -boson and LSP neutralino (right). The color coding is the same as in Figure 1. The branching ratio in the right panel is obtained as $BR(\tilde{t}_1 \rightarrow bW^\pm\tilde{\chi}_1^0) \approx BR(\tilde{t}_1 \rightarrow b\tilde{\chi}_1^\pm) \times BR(\tilde{\chi}_1^\pm \rightarrow W^\pm\tilde{\chi}_1^0)$. As seen from the panels, this stop decay mode can be as high as about 90% or so consistent with the DM constraints for $BR(\tilde{t}_1 \rightarrow t\tilde{\chi}_1^0) \lesssim 10\%$.

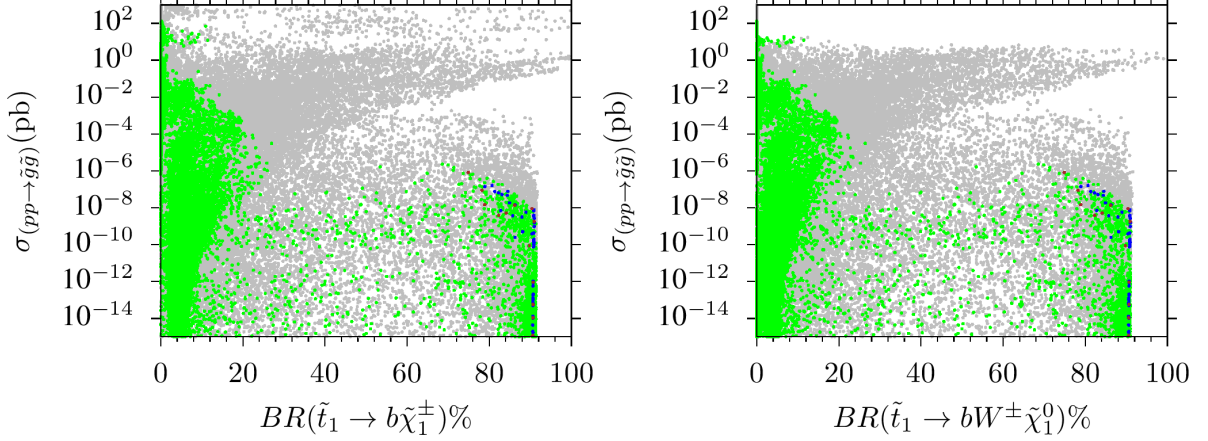


Figure 4: Plots for the gluino pair production cross-section and stop decay channels involving bottom and chargino (left), bottom, W -boson and LSP neutralino (right). The color coding is the same as in Figure 1.

Next we consider these results in terms of the signal strength over the relevant backgrounds which is displayed in Figure 5 in the $m_{\tilde{\chi}_1^0} - m_{\tilde{g}}$ plane. All points are allowed by the current LHC results listed in Section 2. The blue points represent the solutions with $SS \gtrsim 0$, while the black points show those with $SS \gtrsim 2\sigma$, and the red points depict those with $SS \gtrsim 1\sigma$. The rest of the solutions lie in the green region and they yield $SS \gtrsim 3\sigma$. Assuming negative results for gluino searches, one can exclude the solutions represented in red, black and green. The blue points yield $SS \gtrsim 0$, which means the $\tilde{g} \rightarrow \tilde{t}_1 t$ analyses cannot be applied to these points. According to the results shown in Figure 5, one can exclude the gluino mass scales below about 2 TeV with 68% CL, while those below about 1.9 TeV can be excluded up to about 95% CL. Considering an error of about 10% in calculation of the SUSY mass spectrum, these bounds obtained in CMSSM through the gluino pair production, with the gluinos decaying into a stop and top quark, are quite similar to those obtained in the low scale analyses.

Another possibility is for the gluinos to decay into a LSP neutralino along with a pair of top quarks, when the $\tilde{g} \rightarrow \tilde{t}_1 t$ process is not available. Figure 6 displays the results for this case with the plots in the $\sigma(pp \rightarrow \tilde{g}\tilde{g}) - BR(\tilde{g} \rightarrow \tilde{t}\tilde{t}\tilde{\chi}_1^0)$ and $m_{\tilde{\chi}_1^0} - m_{\tilde{g}}$ planes. The color coding in the left panel is the same as in Figure 1, while the right panel is represented in terms of SS , whose color coding is the same as in Figure 5. The exclusion region for the gluino mass scale can be slightly lowered through this channel as the regions with $m_{\tilde{g}} \lesssim 1.6$ TeV are excluded up to about 68% CL, while those with $m_{\tilde{g}} \lesssim 1.4$ TeV are excluded up to about 95% CL.

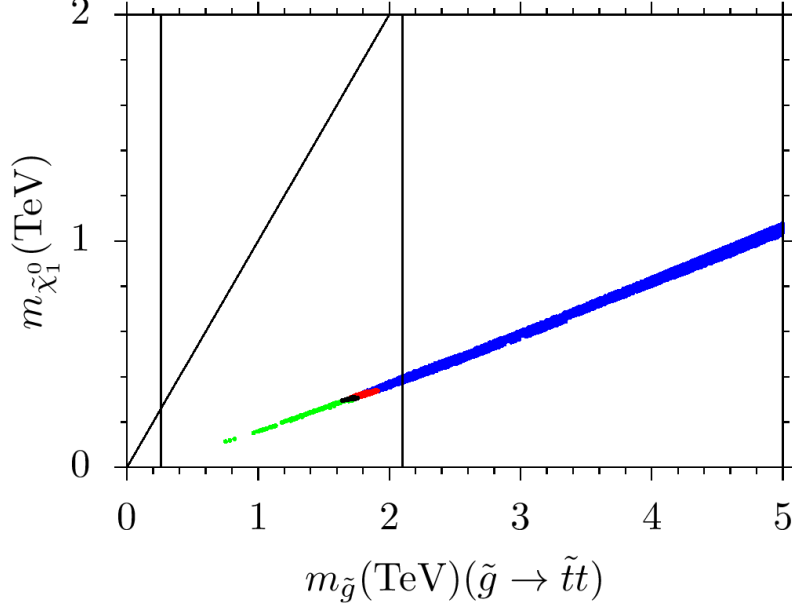


Figure 5: LSP neutralino and gluino masses in terms of the signal significance for $\tilde{g} \rightarrow \tilde{t}_1 t$. All points are allowed by the current LHC results listed in Section 2. Blue points represent the solutions with $SS \gtrsim 0$, the black points show those with $SS \gtrsim 2\sigma$, and red points depict those with $SS \gtrsim 1\sigma$. The remaining solutions in the green region yield $SS \gtrsim 3\sigma$.

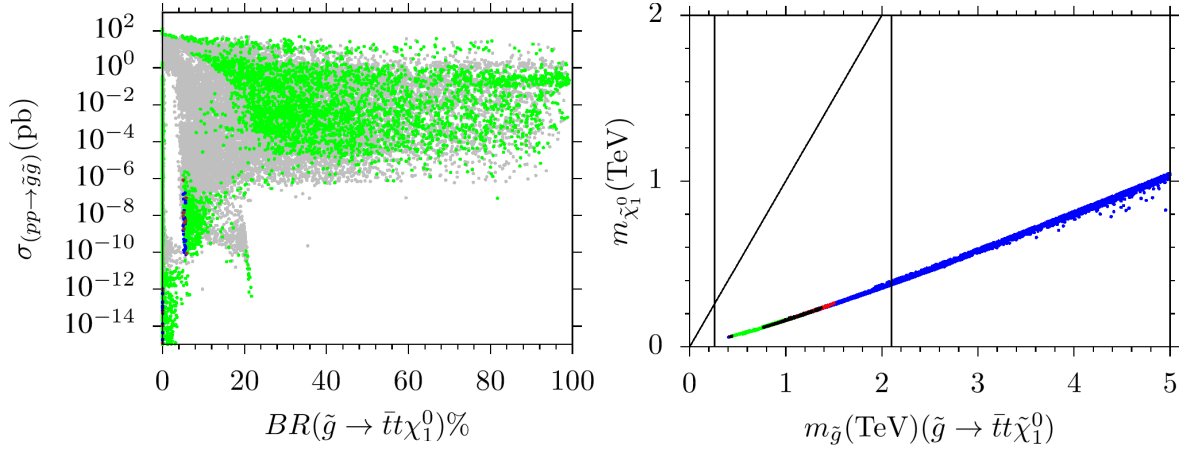


Figure 6: Plots in the $\sigma(pp \rightarrow \tilde{g}\tilde{g}) - \text{BR}(\tilde{g} \rightarrow \tilde{t}\tilde{\chi}_1^0)$ and $m_{\tilde{\chi}_1^0} - m_{\tilde{g}}$ planes. The color coding in the left panel is the same as in Figure 1, while the right panel is represented in terms of SS , whose color coding is the same as in Figure 5.

4 Gluino Exclusion in NUGM

In this section we relax the universality in the gaugino sector by setting all gaugino masses independent of each other such that the linear correlation between the LSP neutralino and gluino masses does not hold. Non-universality in SUSY GUTs can be realized in several cases without conflicting with the underlying GUT symmetry and gauge coupling unification using non-singlet F -terms with non-zero VEVs [43], or F -terms which are a linear combination of two or more distinct fields from different representations [44].

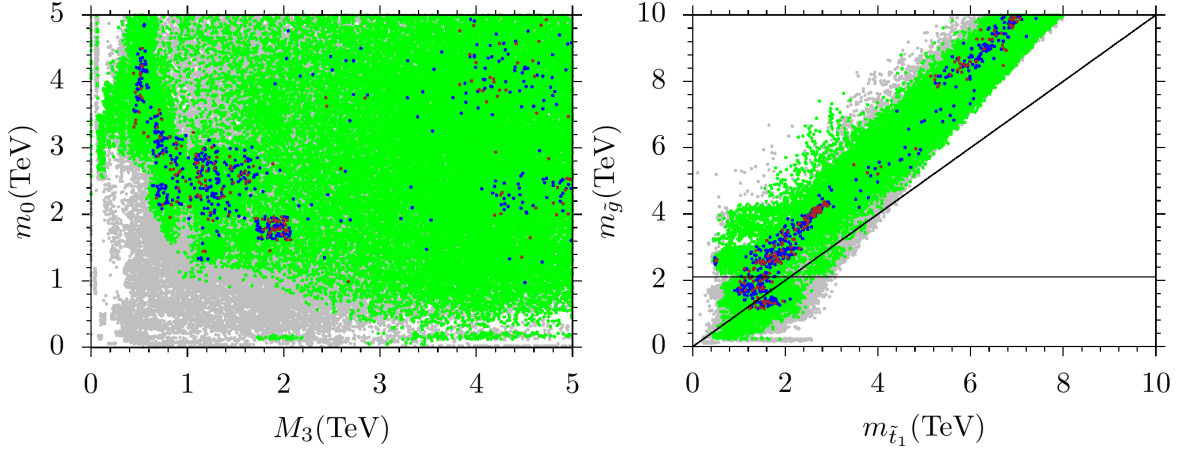


Figure 7: Plots in the $m_0 - M_3$ and $m_{\tilde{g}} - m_{\tilde{t}_1}$ planes. The color coding is the same as in Figure 1. The diagonal line in the right panel indicates the mass degeneracy between the gluino and stop.

Another way is to assume two distinct sources of SUSY breaking [45].

We first display our results for the scalar and gaugino masses in terms of the GUT parameters and low scale masses of the stop and gluino in Figure 7 in the $m_0 - M_3$ and $m_{\tilde{g}} - m_{\tilde{t}_1}$ planes. The color coding is the same as in Figure 1. The diagonal line in the right panel indicates the mass degeneracy between the gluino and stop. As seen from the $m_0 - M_3$ plane, the DM constraints do not exclude any region in the fundamental parameter space, even though some regions in gray are excluded by the current LHC results. However, the correlation between the gluino and stop masses still holds as seen from the $m_{\tilde{g}} - m_{\tilde{t}_1}$ plane, since these SUSY particles raise mutually their masses in the RGEs. The $m_{\tilde{g}} - m_{\tilde{t}_1}$ plane shows that the gluino happens to be heavier than the stop in most of the parameter space, while a relatively small portion can yield a stop heavier than the gluino. Moreover, the DM constraints allow the gluino and stop to be as low as about 1 TeV, in contrast to the CMSSM case.

We discuss the low scale mass spectrum in more details with plots in the $m_{\tilde{g}} - m_{\tilde{\chi}_1^0}$, $m_{\tilde{t}_1} - m_{\tilde{\chi}_1^0}$, $m_{\tilde{g}} - m_{\tilde{\chi}_1^\pm}$ and $m_{\tilde{t}_1} - m_{\tilde{\chi}_1^\pm}$ planes of Figure 8. The color coding is the same as in Figure 1, and the diagonal lines indicate the mass degeneracy between the particles involved. The $m_{\tilde{g}} - m_{\tilde{\chi}_1^0}$ plane reveals that the gluino is nearly degenerate with the LSP neutralino for mass scales $1.1 \gtrsim m_{\tilde{g}} \gtrsim 1.5$ TeV. Such solutions favor the gluino-neutralino coannihilation scenarios which are able to bring the thermal relic abundance of the LSP neutralino to the ranges allowed by the WMAP and Planck measurements. Besides, since $m_{\tilde{g}} \approx m_{\tilde{\chi}_1^0}$, these solutions forbid processes $\tilde{g} \rightarrow \tilde{t}_1 t$ and $\tilde{g} \rightarrow \tilde{t} t \tilde{\chi}_1^0$. Indeed, the exclusion limit on the gluino mass is not severe ($m_{\tilde{g}} \gtrsim 800$ GeV) if it happens to be the NLSP. Similarly, we can also identify the stop-neutralino coannihilation solutions with $0.9 \gtrsim m_{\tilde{t}_1} \approx m_{\tilde{\chi}_1^0} \gtrsim 1.5$ TeV, around the diagonal line in the $m_{\tilde{t}_1} - m_{\tilde{\chi}_1^0}$ plot. For these solutions, the constraint on the relic abundance of the LSP neutralino is satisfied through stop-neutralino coannihilation scenario. The bottom panels of Figure 8 show the chargino mass compared to gluino (left) and stop (right). Although the chargino can be as heavy as about 3 TeV, it is always lighter than the gluino and stop, unless the gluino and/or stop are NLSP.

In addition to gluino and stop, we present the mass spectrum in the $m_{\tilde{\tau}_1} - m_{\tilde{\chi}_1^0}$ and

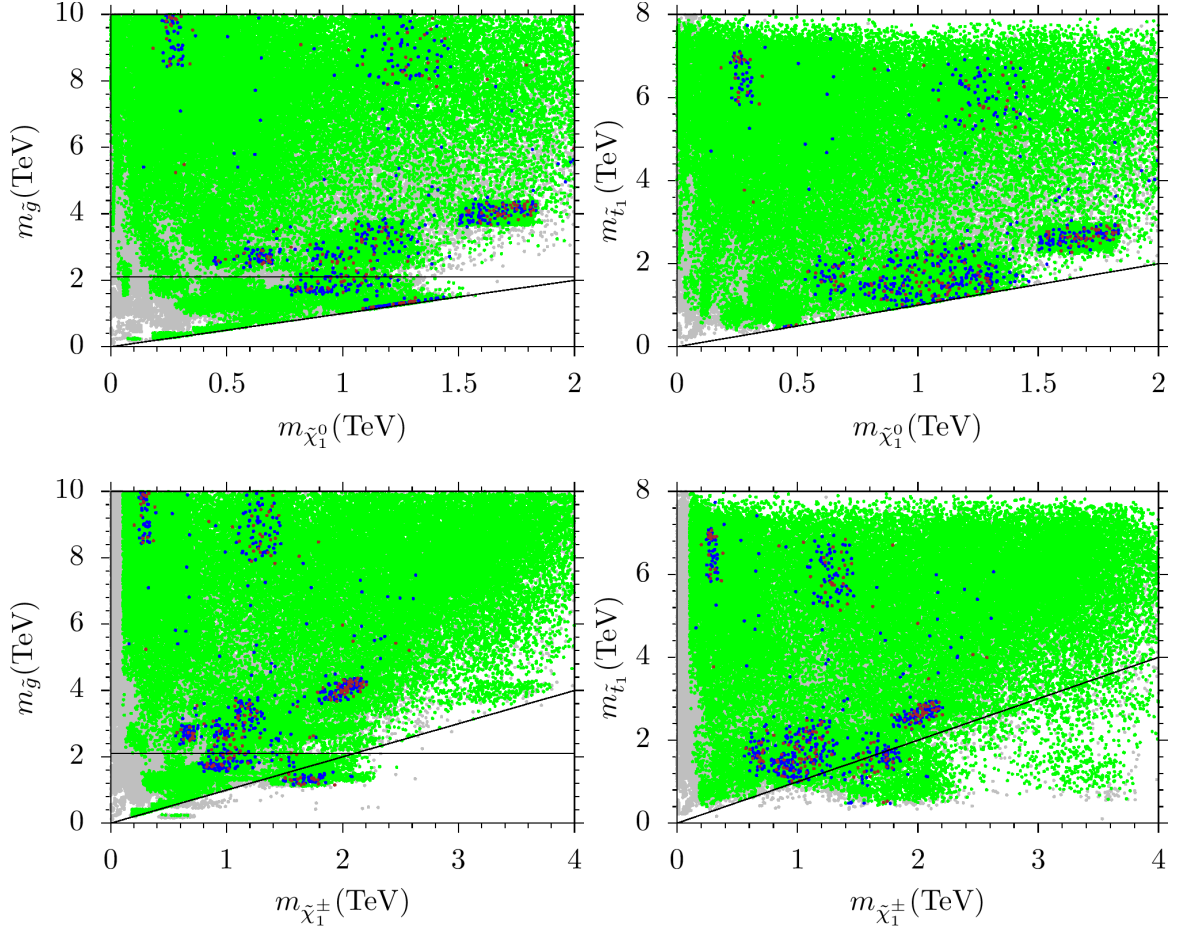


Figure 8: Plots for the mass spectrum in the $m_{\tilde{g}} - m_{\tilde{\chi}_1^0}$, $m_{\tilde{t}_1} - m_{\tilde{\chi}_1^0}$, $m_{\tilde{g}} - m_{\tilde{\chi}_1^\pm}$ and $m_{\tilde{t}_1} - m_{\tilde{\chi}_1^\pm}$ planes. The color coding is the same as in Figure 1, and the diagonal lines indicate the degeneracy between masses shown.

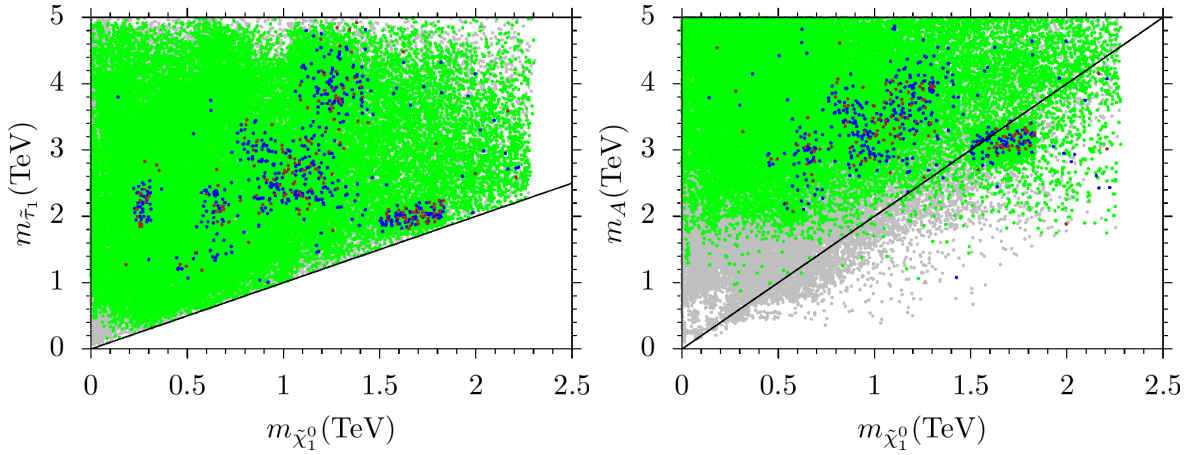


Figure 9: Mass spectrum in the $m_{\tilde{\tau}_1} - m_{\tilde{\chi}_1^0}$ and $m_A - m_{\tilde{\chi}_1^0}$ planes. The color coding is the same as in Figure 1. The diagonal line in the left panel displays the region with $m_{\tilde{\tau}_1} = m_{\tilde{\chi}_1^0}$, while it represents $m_A = 2m_{\tilde{\chi}_1^0}$ in the right panel.

$m_A - m_{\tilde{\chi}_1^0}$ planes. The color coding is the same as in Figure 1. The diagonal line in the left panel indicates the regions with $m_{\tilde{\tau}_1} = m_{\tilde{\chi}_1^0}$, while it represents $m_A = 2m_{\tilde{\chi}_1^0}$ in the right panel. It shows that the stau can be as heavy as about 2.2 TeV, and it is degenerate with the LSP neutralino to within 10% for $1.5 \lesssim m_{\tilde{\tau}_1} \sim m_{\tilde{\chi}_1^0} \lesssim 1.9$ TeV. The solutions in this mass scale favor the stau-neutralino coannihilation scenario in satisfying the constraint on the relic abundance of the LSP neutralino. This mass scale also favors the A -resonance solution as shown in the $m_A - m_{\tilde{\chi}_1^0}$ plane.

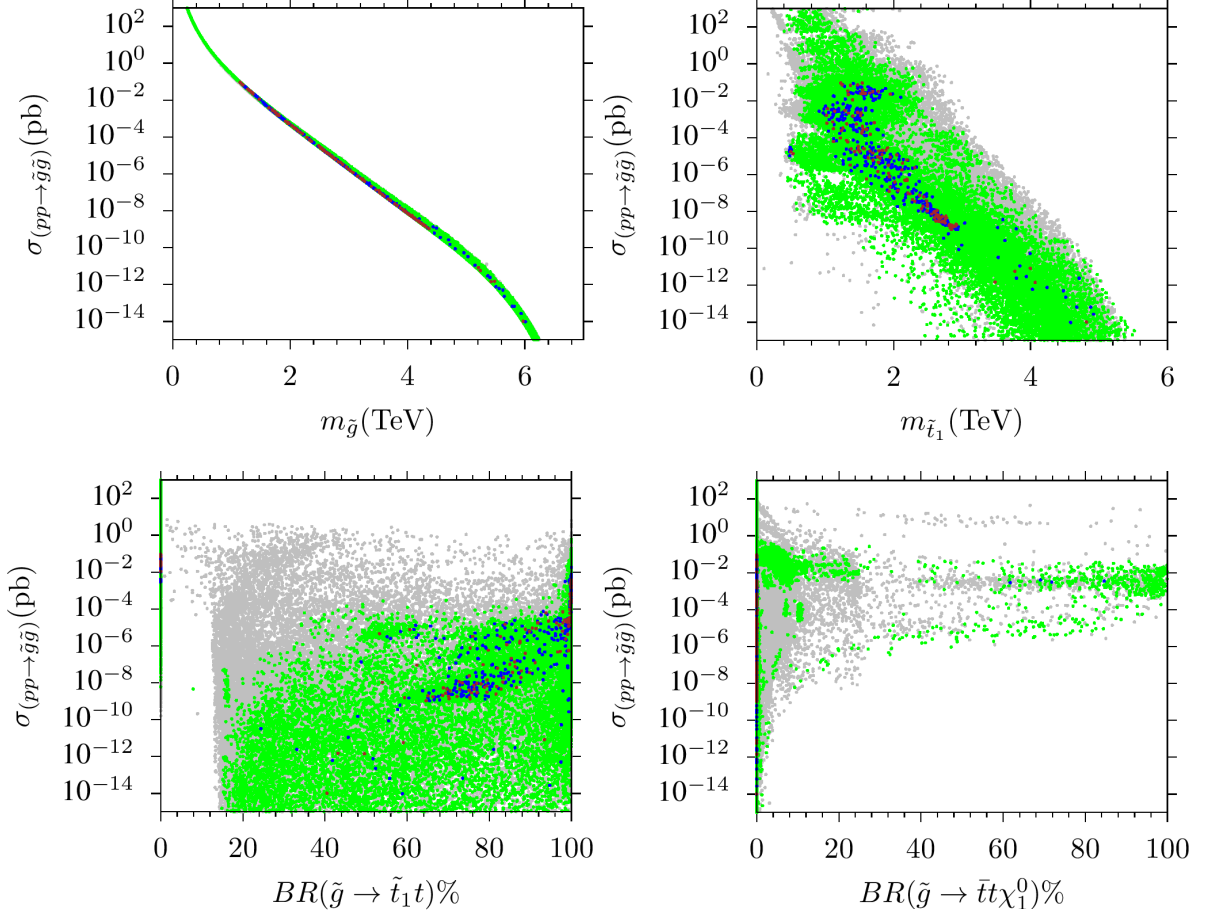


Figure 10: Plots for gluino pair production cross-section and its decay modes in the $\sigma(pp \rightarrow \tilde{g}\tilde{g}) - m_{\tilde{g}}$, $\sigma(pp \rightarrow \tilde{g}\tilde{g}) - m_{\tilde{t}_1}$, $\sigma(pp \rightarrow \tilde{g}\tilde{g}) - \text{BR}(\tilde{g} \rightarrow \tilde{t}_1 t)$ and $\text{BR}(\tilde{g} \rightarrow t\bar{t}\tilde{\chi}_1^0)$ planes. The color coding is the same as in Figure 1.

Figure 10 shows our results for the gluino pair production cross section at 14 TeV and its decay modes in the $\sigma(pp \rightarrow \tilde{g}\tilde{g}) - m_{\tilde{g}}$, $\sigma(pp \rightarrow \tilde{g}\tilde{g}) - m_{\tilde{t}_1}$, $\sigma(pp \rightarrow \tilde{g}\tilde{g}) - \text{BR}(\tilde{g} \rightarrow \tilde{t}_1 t)$ and $\text{BR}(\tilde{g} \rightarrow t\bar{t}\tilde{\chi}_1^0)$ planes. The color coding is the same as in Figure 1. The results are quite similar to those obtained in the CMSSM framework. This is because the particle dynamics remain the same, since we do not extend the particle content and/or the symmetry group. The gluino pair production cross-section can be of the order $\mathcal{O}(100)$ pb for light gluino solutions, while the DM constraints lower it to about 10^{-1} pb by bounding the gluino mass at about 1 TeV from below. The cross-section drops below 10^{-5} pb for $m_{\tilde{g}} \gtrsim 3$ TeV, beyond which the gluino pair production becomes unlikely. Similar discussion can be followed for the stop mass considered as shown in the $\sigma(pp \rightarrow \tilde{g}\tilde{g}) - m_{\tilde{t}_1}$ plot. The $\sigma(pp \rightarrow$

$\tilde{g}\tilde{g}) - \text{BR}(\tilde{g} \rightarrow \tilde{t}_1 t)$ plane shows that the gluino can decay 100% into a stop and top quark consistent with the LHC constraints and DM measurements. The $\tilde{g} \rightarrow \bar{t}t\tilde{\chi}_1^0$ process can also be realized at 100%, but the DM constraints mostly exclude this process. We should note that there are a few solutions satisfying the DM constraints for $\text{BR}(\tilde{g} \rightarrow \bar{t}t\tilde{\chi}_1^0) \lesssim 85\%$. The number of such solutions can increase in a more thorough statistical distribution¹.

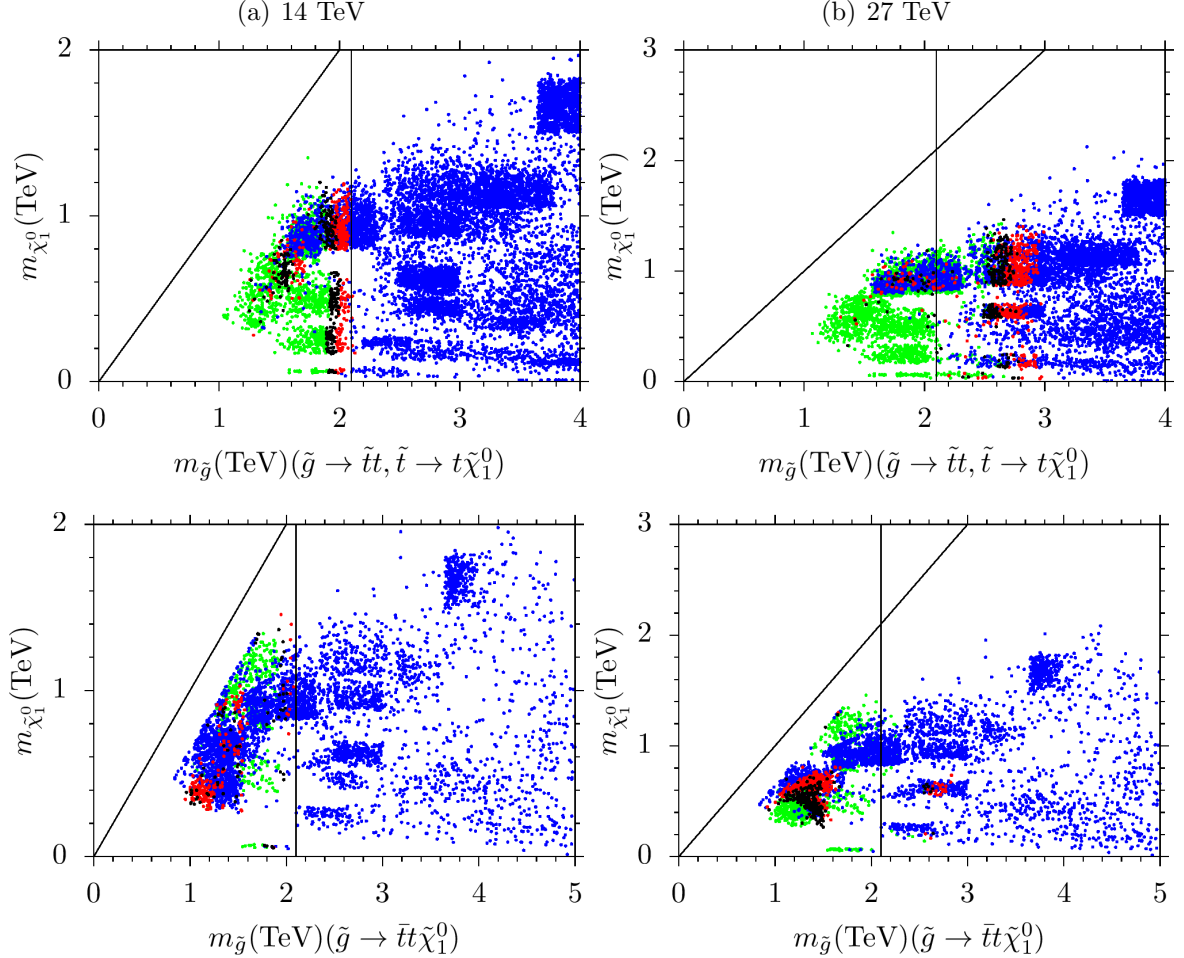


Figure 11: LSP neutralino and gluino masses in terms of the signal significance for the $\tilde{g} \rightarrow \tilde{t}_1 t$ and $\tilde{g} \rightarrow \bar{t}t\tilde{\chi}_1^0$. The color coding is the same as in Figure 5.

Assuming negative results in search of the gluino and/or stop at 14 and 27 TeV, the excluded regions are shown for the $\tilde{g} \rightarrow \tilde{t}_1 t$ and $\tilde{g} \rightarrow \bar{t}t\tilde{\chi}_1^0$ in the LSP neutralino and gluino mass plane of Figure 11 in terms of the signal significance. The color coding is the same as in Figure 5. The top left panel reveals exclusion plots quite similar to those from the ATLAS and CMS experiments with a gluino mass scale lower than about 2 TeV excluded if the gluino decays into a stop and a top quark. This procedure can probe the gluino mass up to about 3 TeV if the center of mass energy is raised to 27 GeV, as seen from the top right panel. The analyzes for the case of Signal3 also yields similar exclusion plots as shown in the bottom panels. Gluino masses below about 2.1 TeV are excluded for 14 TeV, while 27 TeV can exclude regions with $m_{\tilde{g}} \lesssim 3$ TeV. Note that the NLSP gluino solutions

¹Our distribution is also poor in regard to analyzing Signal2, but based on the results from CMSSM, we can expect an exclusion similar to that obtained in the case of Signal1.

have disappeared from the planes of Figure 11 due to the conditions $\sigma(\text{Signal1}) > 0$ in the top panels, and $\sigma(\text{Signal3}) > 0$ in the bottom panels.

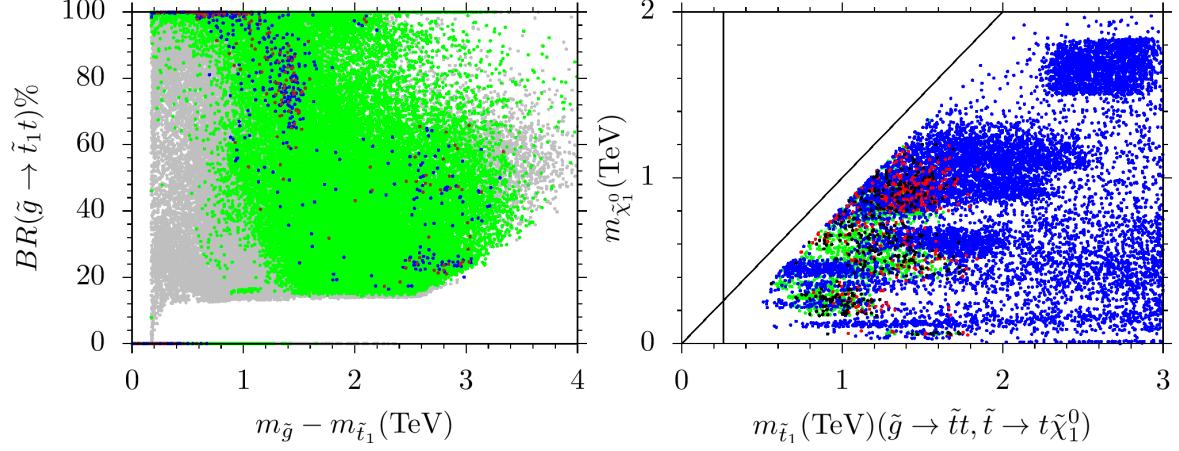


Figure 12: Plots in the $\text{BR}(\tilde{g} \rightarrow \tilde{t}_1 t) - (m_{\tilde{g}} - m_{\tilde{t}_1})$ and $m_{\tilde{\chi}_1^0} - m_{\tilde{t}_1}$ planes. The color coding in the left panel is the same as Figure in 1, while the right panel is obtained with the color coding used in Figure 5.

In addition to gluino and LSP neutralino, the decay mode $\tilde{g} \rightarrow \tilde{t}_1 t$ is also sensitive to the stop mass, and it leads to interesting results regarding the stop mass. This is because a SUSY particle exhibits a strong tendency to decay into the next SUSY particle in the mass spectrum, if it is allowed. If the stop is the heaviest sparticle after gluino in the mass spectrum, the gluino has a strong tendency to decay into a stop as seen from the plots in the $\text{BR}(\tilde{g} \rightarrow \tilde{t}_1 t) - (m_{\tilde{g}} - m_{\tilde{t}_1})$ and $m_{\tilde{\chi}_1^0} - m_{\tilde{t}_1}$ planes of Figure 12. The color coding in the left panel is the same as in Figure 1, while the right panel is obtained with the color coding used in Figure 5. The $\text{BR}(\tilde{g} \rightarrow \tilde{t}_1 t) - (m_{\tilde{g}} - m_{\tilde{t}_1})$ plane shows that $\text{BR}(\tilde{g} \rightarrow \tilde{t}_1 t) \sim 100\%$ for $m_{\tilde{g}} - m_{\tilde{t}_1} \lesssim 1$ TeV, and even though it is possible to obtain a large branching fraction for $m_{\tilde{g}} - m_{\tilde{t}_1} \sim 2$ TeV, such solutions correspond to a heavy gluino, whose pair production becomes unlikely. The $m_{\tilde{\chi}_1^0} - m_{\tilde{t}_1}$ plot summarizes our discussion for the decay $\tilde{g} \rightarrow \tilde{t}_1 t$ with the stop subsequently decaying into a top quark and a LSP neutralino. According to the results shown in this plane, the stop mass up to about 1.8 TeV can be excluded, if the collider analyses do not yield any direct signal up to this mass scale.

Before concluding we summarize our findings in Figure 13 in the $m_{\tilde{\chi}_1^0} - m_{\tilde{g}}$ and $m_{\tilde{\chi}_1^0} - m_{\tilde{t}_1}$ planes, with the color coding is the same as in Figure 1. The orange curve represents the exclusion region at 14 TeV, while the dark green and the red curves are obtained for 27 TeV and 100 TeV respectively. The solutions with $m_{\tilde{g}} \lesssim 2$ TeV are excluded in the current LHC run, while the HE-LHC (at 27 TeV) and FCC (at 100 TeV) can probe a gluino mass up to about 3 TeV and 6 TeV respectively. Comparing with Figure 9 the exclusion regions from 14 TeV and 27 TeV do not yield any impact on the stau-neutralino coannihilation and A -resonance solutions, while 100 TeV can probe and exclude them in case of no direct signal in near future. Besides, the analyses for the $\tilde{g} \rightarrow \tilde{t}_1 t$ decay mode cannot be applied if the gluino happens to be NLSP (brown and blue points around the diagonal line in the left panel). Furthermore, the decay mode $\tilde{g} \rightarrow \tilde{t}_1 t$ can probe the stop up to about 1.8 TeV, 2.5 TeV and 4.4 TeV in the experiments at 14 TeV, 27 TeV and 100 TeV center of mass energies respectively, as shown in the $m_{\tilde{\chi}_1^0} - m_{\tilde{t}_1}$ plane.

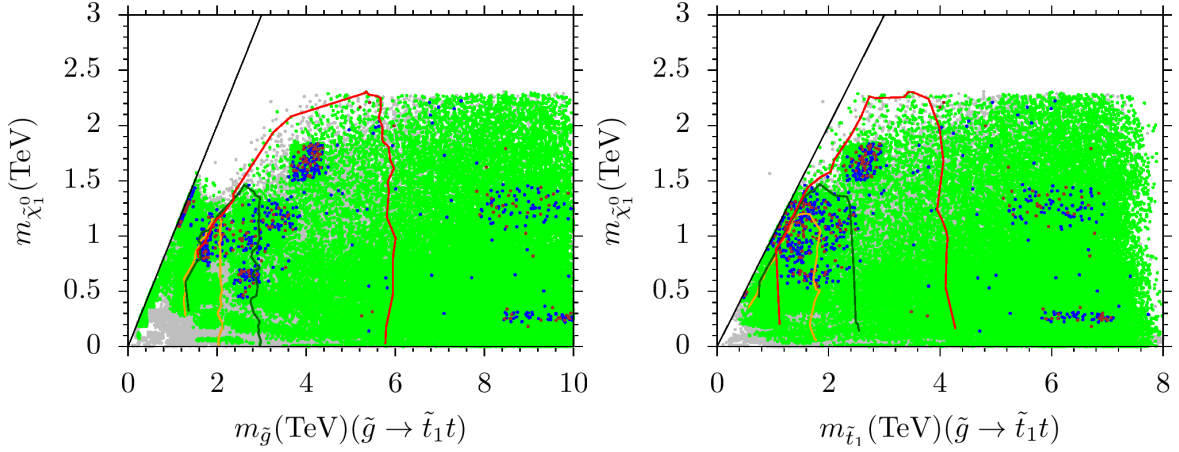


Figure 13: Summary of our findings in the $m_{\tilde{\chi}_1^0} - m_{\tilde{g}}$ and $m_{\tilde{\chi}_1^0} - m_{\tilde{t}_1}$ planes. The color coding is the same as in Figure 1. The orange curve represents the exclusion at 14 TeV, while the dark green and the red curves are obtained for 27 TeV and 100 TeV respectively.

We should note that the curves represented in Figure 13 can be interpreted as the minimum reach of the future experiments, since we set the luminosity to 36.1 fb^{-1} in our analyses. It has already been reported that the FCC can probe the gluino mass up to about 10 TeV (see, for instance, [42]) for an integrated luminosity of 3000 fb^{-1} . Figure 14 displays our results in probing gluino at the FCC experiments if the 3000 fb^{-1} luminosity is reached. One can expect that a gluino mass up to about 9-10 TeV will be probed, and we remain optimistic that a direct signal will sight the gluino in the near future.

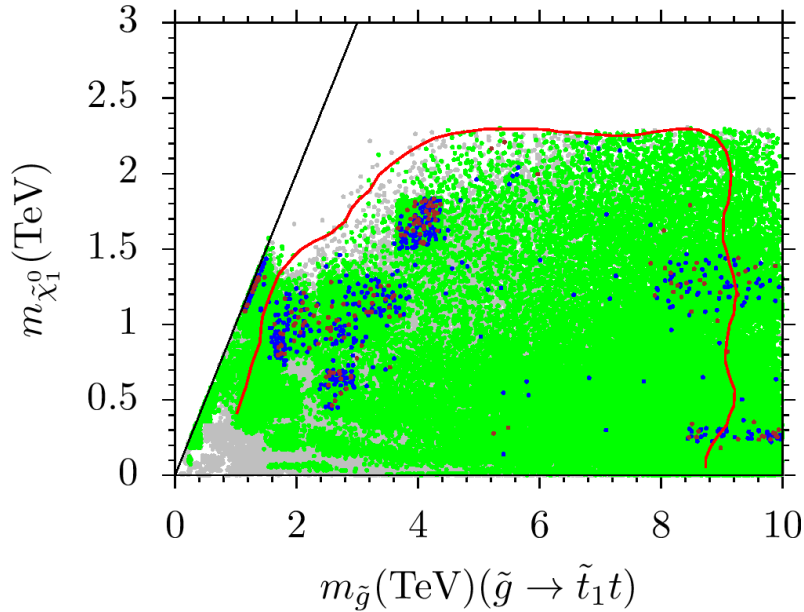


Figure 14: Gluino probe at the FCC with 100 TeV center of mass energy. The color coding is the same in Figure 1. The red curve represents the gluino reach when the luminosity is set to 3000 fb^{-1} .

5 Conclusion

We have explored gluino masses in the CMSSM and NUGM frameworks through its decay into a stop and a top quark, or into a pair of top quarks along with a LSP neutralino. We find that the region with $m_{\tilde{g}} \lesssim 2$ TeV is excluded up to 68% CL in the CMSSM if the gluino decays into a stop and top quark. The 95% CL exclusion is also quite significant, since it requires $m_{\tilde{g}} \gtrsim 1.9$ TeV. Considering an error of about 10% in the calculation of the SUSY mass spectrum, such exclusion bounds on the gluino mass more or less overlap with the current LHC results. The decay mode $\tilde{g} \rightarrow \bar{t}t\tilde{\chi}_1^0$ may take over if the $\tilde{g} \rightarrow \tilde{t}_1t$ is not allowed. One can probe in this case a gluino mass up to about 1.5 TeV with 68% CL in the CMSSM, and about 1.4 TeV with 95% CL. Imposing the DM constraints yield a lower bound on the gluino and stop masses of about 3.2 TeV, which is beyond the reach of the current LHC experiments.

We performed a similar analyses in the NUGM framework corresponding to non-universal gaugino masses at GUT scale. Non-universality in the gaugino sector breaks the linear correlation between the gluino and LSP neutralino masses so that one can identify solutions corresponding to the gluino-neutralino coannihilation scenario. Even though the DM constraints have a strong impact also in the NUGM parameter space, it is not as strong as that in CMSSM, and a lower bound on the gluino and stop masses is about 1 TeV. An NLSP gluino is realized in the mass region $1.1 \lesssim m_{\tilde{g}} \approx m_{\tilde{\chi}_1^0} \lesssim 1.5$ TeV. Since the mass difference between the gluino and LSP neutralino is rather small, these solutions cannot be probed through a gluino decay into a stop and top quark. Indeed, the exclusion region in this case from the LHC, namely $m_{\tilde{g}} \gtrsim 800$ GeV, is not very severe. In NUGM we identify stop-neutralino coannihilation solutions with $m_{\tilde{t}_1} \approx m_{\tilde{\chi}_1^0} \in [0.9 - 1.5]$ TeV and stau-neutralino coannihilation for $1.5 \lesssim m_{\tilde{\tau}} \lesssim 2$ TeV and A -resonance solutions for $2.5 \lesssim m_A \lesssim 3$ TeV. We find that the a gluino of mass up to about 2 TeV can be excluded through the decay mode $\tilde{g} \rightarrow \tilde{t}_1t$ at 14 TeV, and it can be probed up to about 3 TeV and 6 TeV at the HE-LHC and FCC experiments respectively, with an integrated luminosity of 36.1 fb^{-1} . We also note that a 100 TeV FCC can probe gluino masses up to about 9-10 TeV with an integrated luminosity of 3000 fb^{-1} .

Finally, experiments at 100 TeV center of mass energy can also probe the stau-neutralino coannihilation and A -resonance solutions. Besides the gluino, the impact on the stop mass through the $\tilde{g} \rightarrow \tilde{t}_1t$ channel is significant as it can be probed up to about 1.8 TeV, 2.5 TeV and 4.4 TeV in experiments with 14 TeV, 27 TeV and 100 TeV center of mass energies respectively.

6 Acknowledgments

The work of Z. A, Z. K. and C. S. U is supported by the Scientific and Technological Research Council of Turkey (TUBITAK) Grant no. MFAG-118F090. Q. S. is supported in part by DOE under Grant no. DE-SC 0013880. CSU also would like to thank the Physics and Astronomy Department and Bartol Research Institute of the University of Delaware, for kind hospitality where part of this work has been done. Part of the calculations reported in this paper were performed at the National Academic Network and Information Center (ULAKBIM) of TUBITAK, High Performance and Grid Computing Center (TRUBA Resources).

References

- [1] B. Ananthanarayan, G. Lazarides and Q. Shafi, Phys. Rev. D **44**, 1613 (1991) and Phys. Lett. B **300**, 24 (1993)5; Q. Shafi and B. Ananthanarayan, Trieste HEP Cosmol.1991:233-244;
- [2] V. Barger, M. Berger and P. Ohmann, Phys. Rev. D **49**, (1994) 4908; M. Carena, M. Olechowski, S. Pokorski and C. Wagner, Nucl. Phys. B **426**, 269 (1994); B. Ananthanarayan, Q. Shafi and X. Wang, Phys. Rev. D **50**, 5980 (1994); G. Anderson et al. Phys. Rev. D **47**, (1993) 3702 and Phys. Rev. D **49**, 3660 (1994); R. Rattazzi and U. Sarid, Phys. Rev. D **53**, 1553 (1996); T. Blazek, M. Carena, S. Raby and C. Wagner, Phys. Rev. D **56**, 6919 (1997); T. Blazek, S. Raby and K. Tobe, Phys. Rev. D **62**, 055001 (2000); H. Baer, M. Diaz, J. Ferrandis and X. Tata, Phys. Rev. D **61**, 111701 (2000); H. Baer, M. Brhlik, M. Diaz, J. Ferrandis, P. Mercadante, P. Quintana and X. Tata, Phys. Rev. D **63**, 015007(2001); S. Profumo, Phys. Rev. D **68** (2003) 015006; C. Balazs and R. Dermisek, JHEP **0306**, 024 (2003); C. Pallis, Nucl. Phys. B **678**, 398 (2004); M. Gomez, G. Lazarides and C. Pallis, Phys. Rev. D **61** (2000) 123512, Nucl. Phys. B **638**, 165 (2002) and Phys. Rev. D **67**, 097701(2003); I. Gogoladze, Y. Mimura, S. Nandi and K. Tobe, Phys. Lett. B **575**, 66 (2003); U. Chattopadhyay, A. Corsetti and P. Nath, Phys. Rev. D **66** 035003, (2002); T. Blazek, R. Dermisek and S. Raby, Phys. Rev. Lett. **88**, 111804 (2002) and Phys. Rev. D **65**, 115004 (2002); M. Gomez, T. Ibrahim, P. Nath and S. Skadhauge, Phys. Rev. D **72**, 095008 (2005); K. Tobe and J. D. Wells, Nucl. Phys. B **663**, 123 (2003); W. Altmannshofer, D. Guadagnoli, S. Raby and D. M. Straub, Phys. Lett. B **668**, 385 (2008); D. Guadagnoli, S. Raby and D. M. Straub, JHEP **0910**, 059 (2009); H. Baer, S. Kraml and S. Sekmen, JHEP **0909**, 005 (2009); K. Choi, D. Guadagnoli, S. H. Im and C. B. Park, arXiv:1005.0618 [hep-ph]; B. Dutta and Y. Mimura, arXiv:1810.08413 [hep-ph]; S. Raza, Q. Shafi and C. S. n, Phys. Rev. D **92**, no. 5, 055010 (2015) [arXiv:1412.7672 [hep-ph]].
- [3] U. Chattopadhyay and P. Nath, Phys. Rev. D **65**, 075009 (2002); S. Komine and M. Yamaguchi, Phys. Rev. D **65**, 075013 (2002); S. Profumo, Phys. Rev. D **68**, 015006 (2003); C. Pallis, Nucl. Phys. B **678**, 398 (2004); C. Balazs and R. Dermisek, JHEP **0306**, 024 (2003); W. Altmannshofer, D. Guadagnoli, S. Raby and D. M. Straub, Phys. Lett. B **668**, 385 (2008); I. Gogoladze, R. Khalid, N. Okada and Q. Shafi, Phys. Rev. D **79**, 095022 (2009); S. Antusch and M. Spinrath, Phys. Rev. D **79**, 095004 (2009); H. Baer, I. Gogoladze, A. Mustafayev, S. Raza and Q. Shafi, JHEP **1203**, 047 (2012) [arXiv:1201.4412 [hep-ph]]; I. Gogoladze, R. Khalid, S. Raza and Q. Shafi, JHEP **1012**, 055 (2010) [arXiv:1008.2765 [hep-ph]]; S. Raza, Q. Shafi and C. S. Un, JHEP **1905**, 046 (2019) [arXiv:1812.10128 [hep-ph]].
- [4] P. Langacker and J. Wang, Phys. Rev. D **58**, 115010 (1998) [hep-ph/9804428]; S. M. Barr, Phys. Rev. Lett. **55**, 2778 (1985); doi:10.1103/PhysRevLett.55.2778 J. L. Hewett and T. G. Rizzo, Phys. Rept. **183** (1989) 193; doi:10.1016/0370-1573(89)90071-9 M. Cvetič and P. Langacker, Phys. Rev. D **54**, 3570 (1996) doi:10.1103/PhysRevD.54.3570 [hep-ph/9511378]; G. Cleaver, M. Cvetič, J. R. Espinosa, L. L. Everett and P. Langacker, Phys. Rev. D **57**, 2701 (1998) doi:10.1103/PhysRevD.57.2701 [hep-ph/9705391]; G. Cleaver, M. Cvetič, J. R. Espinosa, L. L. Everett and P. Langacker, Nucl. Phys. B **525**, 3 (1998)

- doi:10.1016/S0550-3213(98)00277-6 [hep-th/9711178]; D. M. Ghilencea, L. E. Ibanez, N. Irges and F. Quevedo, *JHEP* **0208**, 016 (2002) doi:10.1088/1126-6708/2002/08/016 [hep-ph/0205083]; S. F. King, S. Moretti and R. Nevzorov, *Phys. Rev. D* **73**, 035009 (2006) doi:10.1103/PhysRevD.73.035009 [hep-ph/0510419]; R. Diener, S. Godfrey and T. A. W. Martin, arXiv:0910.1334 [hep-ph]; P. Langacker, *Rev. Mod. Phys.* **81**, 1199 (2009) doi:10.1103/RevModPhys.81.1199 [arXiv:0801.1345 [hep-ph]];
- [5] M. Aaboud *et al.* [ATLAS Collaboration], *Phys. Rev. D* **97**, no. 11, 112001 (2018) doi:10.1103/PhysRevD.97.112001 [arXiv:1712.02332 [hep-ex]]; M. Aaboud *et al.* [ATLAS Collaboration], *Phys. Rev. D* **96**, no. 11, 112010 (2017) doi:10.1103/PhysRevD.96.112010 [arXiv:1708.08232 [hep-ex]].
- [6] T. A. Vami [ATLAS and CMS Collaborations], arXiv:1909.11753 [hep-ex].
- [7] A. Çiçi, Z. Krca and C. S. Ün, *Eur. Phys. J. C* **78**, no. 1, 60 (2018) doi:10.1140/epjc/s10052-018-5549-y [arXiv:1611.05270 [hep-ph]].
- [8] M. LeBlanc [ATLAS Collaboration], *PoS DIS 2018*, 078 (2018); M. Aaboud *et al.* [ATLAS Collaboration], *Phys. Rev. D* **99**, no. 1, 012009 (2019) [arXiv:1808.06358 [hep-ex]]; M. Aaboud *et al.* [ATLAS Collaboration], *Phys. Rev. D* **97**, no. 11, 112001 (2018) [arXiv:1712.02332 [hep-ex]].
- [9] G. Aad *et al.* [ATLAS Collaboration], *Phys. Rev. D* **94**, no. 3, 032003 (2016) doi:10.1103/PhysRevD.94.032003 [arXiv:1605.09318 [hep-ex]].
- [10] The ATLAS collaboration [ATLAS Collaboration], ATLAS-CONF-2013-068.
- [11] Porod, W. *Comput. Phys. Commun.* **2003**, 153, 275.
- [12] Porod, W. and Staub, F. *Comput. Phys. Commun.* **2012** 183, 2458.
- [13] Staub, F. **2008**, *Preprint arXiv:0806.0538*.
- [14] Staub, F. *Comput. Phys. Commun.* **2011** 182, 808.
- [15] Hisano, J.; Murayama, H.; and Yanagida, T. *Nucl. Phys. B* **1993** 402, 46.
- [16] Chkareuli, J. L.; and Gogoladze, I. G. *Phys. Rev. D* **1998** 58, 055011.
- [17] T. E. W. Group [CDF and D0 Collaborations], **2009**, *Preprint arXiv:0903.2503*.
- [18] Gogoladze, I.; Khalid, R.; Raza S.; and Shafi Q. *JHEP* **2011**, 1106, 117.
- [19] Gogoladze, I.; Shafi, Q.; and Un, C. S. *JHEP* **2012** 1208, 028.
- [20] Adeel Ajaib, M.; Gogoladze, I.; Shafi, Q.; and Un, C. S. *JHEP* **2013** 1307, 139.
- [21] Ibanez, L. E.; and Ross, G. G. *Phys. Lett. 110B* **1982** 215.
- [22] Inoue, K.; Kakuto, A.; Komatsu, H.; and Takeshita S., *Prog. Theor. Phys.* **1982** 68, 927.
- [23] Ibanez, L. E. *Phys. Lett.* **1982** 118B, 73.

- [24] Ellis, J. R.; Nanopoulos D. V.; and Tamvakis, K. *Phys. Lett.* **1983** *121B*, 123.
- [25] Alvarez-Gaume, L.; Polchinski, J.; and Wise, M. B. *Nucl. Phys. B* **1983** *221*, 495.
- [26] Nakamura, K. *et al.* [Particle Data Group Collaboration], *J. Phys. G* **2010** *37*, 075021.
- [27] G. Hinshaw *et al.* [WMAP Collaboration], *Astrophys. J. Suppl.* **208**, 19 (2013) [arXiv:1212.5226 [astro-ph.CO]].
- [28] Y. Akrami *et al.* [Planck Collaboration], arXiv:1807.06205 [astro-ph.CO].
- [29] See for instance,
H. Baer, I. Gogoladze, A. Mustafayev, S. Raza and Q. Shafi, *JHEP* **1203**, 047 (2012) doi:10.1007/JHEP03(2012)047 [arXiv:1201.4412 [hep-ph]]; T. Li, D. V. Nanopoulos, S. Raza and X. C. Wang, *JHEP* **1408**, 128 (2014) doi:10.1007/JHEP08(2014)128 [arXiv:1406.5574 [hep-ph]].
- [30] G. Belanger, F. Boudjema, A. Pukhov and A. Semenov, *Comput. Phys. Commun.* **176**, 367 (2007) doi:10.1016/j.cpc.2006.11.008 [hep-ph/0607059]; G. Belanger, F. Boudjema, A. Pukhov and A. Semenov, *Comput. Phys. Commun.* **185**, 960 (2014) doi:10.1016/j.cpc.2013.10.016 [arXiv:1305.0237 [hep-ph]].
- [31] J. Alwall, M. Herquet, F. Maltoni, O. Mattelaer and T. Stelzer, *JHEP* **1106**, 128 (2011) doi:10.1007/JHEP06(2011)128 [arXiv:1106.0522 [hep-ph]].
- [32] Olive, K. A. *et al.* [Particle Data Group Collaboration], *Chin. Phys. C* **2014** *38*, 090001.
- [33] Aaij, R. *et al.* [LHCb Collaboration], *Phys. Rev. Lett.* **2013** *110*, no. 2, 021801.
- [34] Amhis, Y. *et al.* [Heavy Flavor Averaging Group Collaboration], **2012**, *Preprint arXiv:1207.1158*.
- [35] Asner, D. *et al.* [Heavy Flavor Averaging Group Collaboration], **2010** , *Preprint arXiv:1010.1589*.
- [36] M. Bisset, S. Raychaudhuri and D. K. Ghosh, hep-ph/9608421.
- [37] K. Cranmer, doi:10.5170/CERN-2015-001.247, 10.5170/CERN-2014-003.267 arXiv:1503.07622 [physics.data-an].
- [38] Belanger, G.; Boudjema, F.; Pukhov, A.; and Singh, R. K. *JHEP* **2009** *0911*, 026.
- [39] Baer, H.; Kraml, S.; Sekmen, S.; and Summy, H. *JHEP* **2008** *0803*, 056.
- [40] See, for instance,
H. Baer, V. Barger, J. S. Gainer, P. Huang, M. Savoy, D. Sengupta and X. Tata, *Eur. Phys. J. C* **77**, no. 7, 499 (2017) doi:10.1140/epjc/s10052-017-5067-3 [arXiv:1612.00795 [hep-ph]].

- [41] C. Borschensky, M. Krmer, A. Kulesza, M. Mangano, S. Padhi, T. Plehn and X. Portell, *Eur. Phys. J. C* **74**, no. 12, 3174 (2014) doi:10.1140/epjc/s10052-014-3174-y [arXiv:1407.5066 [hep-ph]]
(see also <https://twiki.cern.ch/twiki/bin/view/LHCPhysics/SUSYCrossSections>)
- [42] H. Baer, V. Barger, J. S. Gainer, P. Huang, M. Savoy, H. Serce and X. Tata, *Phys. Lett. B* **774**, 451 (2017) [arXiv:1702.06588 [hep-ph]]; H. Baer, V. Barger, J. S. Gainer, H. Serce and X. Tata, *Phys. Rev. D* **96**, no. 11, 115008 (2017) [arXiv:1708.09054 [hep-ph]].
- [43] B. Ananthanarayan, P. N. Pandita, *Int. J. Mod. Phys. A* **22**, 3229-3259 (2007); S. Bhattacharya, A. Datta and B. Mukhopadhyaya, *JHEP* **0710**, 080 (2007); S. P. Martin, *Phys. Rev. D* **79**, 095019 (2009); J. Chakraborty and A. Raychaudhuri, *Phys. Lett. B* **673**, 57 (2009).
- [44] S. P. Martin, arXiv:1312.0582 [hep-ph].
- [45] A. Anandakrishnan and S. Raby, *Phys. Rev. Lett.* **111**, 211801 (2013); S. Raza, Q. Shafi and C. S. Un, arXiv:1812.10128 [hep-ph], and references therein.